Journal of Solid State Chemistry 182 (2009) 517–524

Contents lists available at ScienceDirect

Journal of Solid State Chemistry

journal homepage: www.elsevier.com/locate/jssc

Hydrothermal synthesis, characterization, and photocatalytic properties of Zn_2SnO_4

Xianliang Fu, Xuxu Wang *, Jinlin Long, Zhengxin Ding, Tingjiang Yan, Guoying Zhang, Zizhong Zhang, Huaxiang Lin, Xianzhi Fu *

State Key Laboratory Breeding Base of Photocatalysis, Research Institute of Photocatalysis, Fuzhou University, Fuzhou 350002, PR China

ARTICLE INFO

Article history:
Received 4 June 2008
Received in revised form
17 September 2008
Accepted 2 November 2008
Available online 3 December 2008

Keywords:
Hydrothermal synthesis
Zn_2SnO_4
Photocatalytic activity
H_2 evolution

ABSTRACT

Nanosized Zn_2SnO_4 (ZTO) particles were successfully synthesized by a simple hydrothermal process in water/ethylene glycol mixed solution using amines (ethylamine, *n*-butylamine, *n*-hexylamine, and *n*-octylamine) as mineralizer. The products were characterized by X-ray diffractions (XRD), scanning electron microscopy (SEM), transmission electron microscopy (TEM), and N_2 adsorption. The results indicated that the hydrothermal conditions, such as alkaline concentration (*n*-butylamine), reaction temperature, solvent composition, and the kind of amines, had an important influence on the composition, crystallinity, and morphology of the product. The as-synthesized ZTO samples exhibited high activities and durabilities for photodegradation of methyl orange and the activities were mainly affected by the crystallinities of the samples. A hexagonal-shaped ZTO (H-ZTO) sample was prepared in 0.53 M of *n*-butylamine solution at 180 °C for 20 h and its optical properties were characterized by UV–Vis diffuse reflectance and Photoluminescence (PL) spectra. Furthermore, the photocatalytic H_2 evolution reaction from ethanol aqueous solution over H-ZTO was also investigated.

1. Introduction

The ternary semiconductor Zn_2SnO_4 (ZTO) is known for having high-electron mobility, high-electrical conductivity, and attractive optical properties, all of which make it suitable for application as solar cells [1], gas sensor for detection of humidity and various combustible gases [2,3], negative electrode material for Li-ion battery [4,5], and photocatalyst to degrade organic pollutants [6–8]. In recent years, many methods have been developed to prepare ZTO, such as thermal evaporation [9,10], high-temperature calcination [7,11], sol–gel synthesis [12,13], mechanical grinding [14], and hydrothermal reaction [1,5,6,15–17]. Among these methods, the hydrothermal method has been proved to be a simple and effective way to prepare well-crystallized and phase-pure ZTO which is difficult to obtain by high-temperature solid reactions due to the evaporation of ZnO. However, the hydrothermal preparations were generally performed in an aqueous solution using strong base NaOH as mineralizer [5,6,16,17]. Zeng et al. had reported that the transformation process of ZTO is: precursor $\rightarrow ZnSn(OH)_6 \rightarrow$ ZTO [17]. When NaOH was used as the mineralizer, with the reaction ($2Zn^{2+}+Sn^{4+}+8OH^- \rightarrow Zn_2SnO_4+4H_2O$) proceeding, the solution pH value progressively decreases due to the consumption of OH^-. This pH change facilitates the formation of $ZnSn(OH)_6$, which has been shown to be readily formed and was stable at low-pH and low-reaction temperature [16], and consequently hinders the phase transformation of $ZnSn(OH)_6$ to ZTO. In order to accelerate this transformation to form pure ZTO the reaction parameters must be optimized, such as prolonging the reaction time, increasing the reaction temperature, and the concentration of NaOH [17]. But ZnO is the thermodynamically stable phase in high concentration of NaOH [16,17]. However, if weak base was used, such as amines, instead of NaOH, these two problems could be overcome because the weak base could continuously supply OH^- by hydrolysis during the reaction and stabilize the solution pH value. Furthermore, comparing to strong base, the chance to form ZnO in high concentration of the weak base is rather smaller due to its low-dissociation capacity.

In the present paper nanosized ZTO was fabricated in water/ethylene glycol mixed solvent using amines (ethylamine, *n*-butylamine, *n*-hexylamine, and *n*-octylamine) as an alkaline mineralizer. The influence of *n*-butylamine concentration, reaction temperature, solvent composition, and the kind of amine on the structure, crystallinity, and morphology of the formed samples was systematically studied. The photocatalytic activities of as-prepared samples were assessed by photodegradation of methyl orange (MO) and photocatalytic production H_2 from ethanol aqueous solution because of the interest in using solar

* Corresponding authors. Fax: +86 591 83779251.
E-mail addresses: xwang@fzu.edu.cn (X. Wang), xzfu@fzu.edu.cn (X. Fu).

0022-4596/$ - see front matter Crown Copyright © 2008 Published by Elsevier Inc. All rights reserved.
doi:10.1016/j.jssc.2008.11.029

energy to degradation pollutants [18] or converting it into chemical energy [19].

2. Experimental section

2.1. Preparation and characterization of samples

All reagents were of analytical grade without further purification. The samples were fabricated via a modified method [1]. In a typical experiment, 1.05 g (7.70 mmol) $ZnCl_2$ and 1.35 g (3.85 mmol) $SnCl_4 \cdot 5H_2O$ were added to 50 mL water/ethylene glycol solvent (water/ethylene glycol = 1:1, volume ratio, denoted as W/EG) under magnetic stirring. Then 25 mL of 1.2 M *n*-butylamine aqueous solution was added dropwise to the stirred solution. The final concentration of *n*-butylamine in the solution was 0.4 M. After stirring for 0.5 h, the obtained white slurry was transferred to a 100 mL autoclave and then maintained at 180 °C for 20 h. The product formed at the bottom of the autoclave was centrifuged and rinsed thoroughly with deionized water and ethanol several times. Finally, the product was dried in air at 60 °C for 10 h.

Pt modified ZTO was synthesized by photodeposition method [20]. 0.40 g ZTO was suspended in 140 mL H_2O. Then 0.4 mL H_2PtCl_6 solution (0.01 g Pt/mL) and 5 mL CH_3OH were added to the solution. Photodeposition was performed for 10 h under continuous N_2 sparging and four 4 W UV-lamps (254 nm, Philips, TUV 4 W/G4 T5) were used as the light source. After recovering of powders by centrifuging and rinsing, the sample was dried at 60 °C overnight. The sample color varied from white to dark grey. The Pt content of the sample was estimated to be 1.0 wt% by the precursor feeding.

X-ray diffractions (XRD) of the as-prepared samples were performed on a Bruker D8 Advance X-ray diffractometer with Cu $K\alpha$ radiation. Morphologies were characterized by a scanning electron microscopy (SEM) (Hitachi, S-3000N). Transmission electron microscopy (TEM) images and high-resolution transmission electron microscopy (HRTEM) images were obtained by a JEOL model JEM 2010 EX instrument at the accelerating voltage of 200 kV. The Brunauer–Emmett–Teller (BET) specific surface areas were measured by N_2 adsorption at 77 K on the Micromeritics ASAP 2020. UV–Vis diffuse reflectance spectrum (UV–Vis DRS) was recorded on a Varian Cary 500 Scan UV–Vis-NIR spectrometer with $BaSO_4$ as the background. Photoluminescence (PL) emission spectrum was recorded with an Edinburgh Analytical Instruments FL/FSTCSPC920 equipped with a 150 W xenon lamp as the excitation source at room temperature.

2.2. Photocatalytic reactions

The photocatalytic activities of ZTO were evaluated by the degradation of MO solution and photocatalytic production of H_2 from aqueous ethanol solution. The activities of commercial Degussa P25 TiO_2 (70% anatase and 30% rutile, with a BET surface area ca. 50 m^2/g), commonly considered as a reference for the evaluation of photocatalytic activity, were also measured under the same reaction conditions.

The photodegradation of MO was conducted with a tubular quartz reactor, surrounded by four 4 W UV-lamps with a wavelength centered at 254 nm (Philips, TUV 4 W/G4 T5). In a typical experiment, 50 mg ZTO was added to 200 mL 20 ppm (mg/L) MO aqueous solution and stirred for 1 h before irradiation in order to establish an adsorption–desorption equilibrium. During the experiment a 3 mL solution was withdrawn through a pipette every 20 min and then centrifuged. The absorbance of the clear liquor was measured on a Varian UV–Vis spectrophotometer (Cary-50).

The photocatalytic H_2 evolution reaction was performed in a closed gas circulating system. An inner irradiation type quartz reaction cell with a 125 W high-pressure Hg lamp (Shanghai Yaming Lighting Co., Ltd, GGZ125, with a maximum emission at about 365 nm) was employed. The temperature of the reaction cell was controlled at about 30 °C by circulating water. In a typical experiment, 50 mg ZTO was suspended in 200 mL of aqueous solution containing 5 mL of ethanol. Before the reaction was initiated, the whole reaction system was evacuated by a mechanical pump and then filled with 101 kPa of high-purity N_2 (>99.99%). This process was repeated three times in order to remove the O_2 of the system. The evolved H_2 was circulated in the system by a micro diaphragm gas pump (Germany, NMP-830KNE, KNF Neuberger) and determined every 30 min by an on-line gas chromatograph (Shanghai Precision Scientific Instrument Co., GC112A, TCD, N_2 carrier).

3. Results and discussion

3.1. Effect of hydrothermal conditions on ZTO synthesis

3.1.1. Effect of n-butylamine concentration

The effect of *n*-butylamine concentration on the crystalline phase of the formed samples was investigated with the reactions carried out at 180 °C for 20 h. As demonstrated in Fig. 1, when *n*-butylamine concentration was below 0.27 M (Fig. 1a–c), all of the diffraction peaks were attributed to tetragonal-phase SnO_2 (JCPDS 77-449) and their crystallinities deteriorated with increasing *n*-butylamine concentration. No Zn species diffraction peaks were found in the patterns. When *n*-butylamine concentration was beyond 0.40 M, pure-phase ZTO was obtained (Fig. 1d and e) and the crystallinity was favored at high concentration of 0.53 M (Fig. 1e). These phenomena had also been observed using NaOH as the mineralizer [17].

The effect of NaOH concentration on the hydrothermal synthesis of ZTO has been recently described by Zeng et al. [17]. As *n*-butylamine is a weak base, it would play the same role as NaOH in the hydrothermal process. In this work, at the beginning experiment stage, $ZnCl_2$ and $SnCl_4$ are dissolved and ionized in the

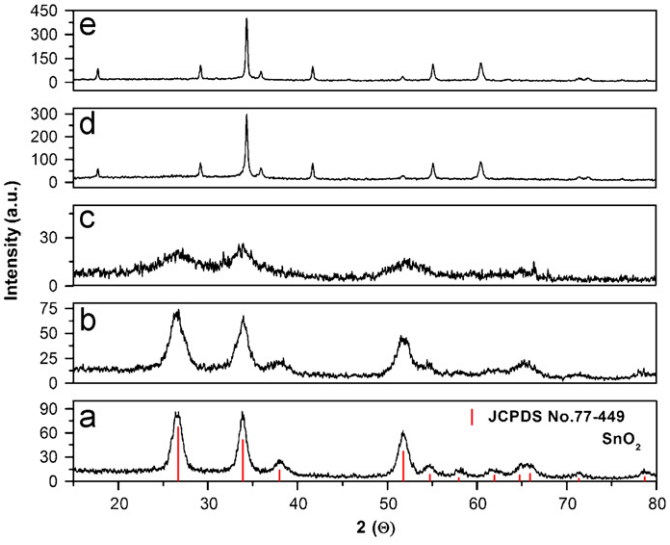

Fig. 1. XRD patterns of the samples synthesized in different concentration of *n*-butylamine: (a) 0 M, (b) 0.13 M, (c) 0.27 M, (d) 0.40 M, and (e) 0.53 M (solvent: W/EG, temperature: 180 °C, time: 20 h).

mixed solvent. When the *n*-butylamine concentration is low ($\leqslant$0.27 M), owing to the strong hydrolysis effect of Sn^{4+}, Eq. (1) occurs and H_2SnO_3 is produced. H_2SnO_3 transforms to SnO_2 through the following hydrothermal process according to Eq. (2). The Zn^{2+} ions are still kept in the solution and wash away after reaction. But with increasing the *n*-butylamine concentration, Eq. (3) dominates the reaction and deteriorates the crystallinity of SnO_2. When *n*-butylamine comes up to an appropriate concentration (0.4 M), ZTO can be formed according to Eqs. (4) and (5). This is mainly due to the fact that the solubility of ZTO is lower than that of other compounds under the reaction conditions. Further increasing the *n*-butylamine concentration to 0.5 M will promote the growth of ZTO and results in higher crystallinity.

$$Sn^{4+} + 3H_2O \rightleftharpoons H_2SnO_3 + 4H^+ \quad (1)$$

$$H_2SnO_3 \rightarrow SnO_2\downarrow + H_2O \quad (2)$$

$$Sn^{4+} + 6OH^- \rightarrow Sn(OH)_6{}^{2-} \quad (3)$$

$$Zn^{2+} + 4OH^- \rightarrow Zn(OH)_4{}^{2-} \quad (4)$$

$$Sn(OH)_6{}^{2-} + 2Zn(OH)_4{}^{2-} \rightarrow Zn_2SnO_4\downarrow + 4H_2O + 6OH^- \quad (5)$$

$$Zn(OH)_4{}^{2-} \rightarrow ZnO\downarrow + H_2O + 2OH^- \quad (6)$$

3.1.2. Effect of hydrothermal temperature

Fig. 2 shows the XRD patterns of the samples synthesized at a temperature between 140 and 200 °C. The dominant phase of the sample synthesized at 140 °C was hexagonal-phase ZnO (JCPDS 89-1397) (Fig. 2a). Increasing the temperature to 160 °C, a mixture phase of ZTO and ZnO was formed (Fig. 2b). It was highly probable that pure ZTO could be obtained at such a temperature by prolonging the reaction time. The samples obtained at 180 °C (Fig. 2c) and 200 °C (Fig. 2d) were cubic-phase ZTO and the crystallinity was significantly improved. All the diffraction peaks of the ZTO were consistent with the JCPDS (74-2184) data of the cubic spinel-structured ZTO with a lattice parameter of 8.65 Å.

Reaction temperature is an important thermodynamical factor for a hydrothermal reaction. As described above, when the *n*-butylamine concentration reaches 0.4 M, the precursors of ZTO are in the form of $Zn(OH)_4^{2-}$ and $Sn(OH)_6^{2-}$. Whether the reaction of Eq. (5) occurs depends on the hydrothermal temperature. When the hydrothermal reaction was carried out at 140 °C, this temperature is insufficient to drive the reaction of Eq. (5), but enough to drive the reaction of Eq. (6) to form ZnO. A higher reaction temperature of 160 °C is clearly required to fabricate ZTO. This temperature is obviously lower than that in literature, where NaOH was used as mineralizer [5,17].

3.1.3. Effect of solvent composition

In order to reveal the advantage of the mixed solvent, two comparison experiments were performed in water and ethylene glycol (EG). When the reaction was conducted in water (Fig. 3a), a mixture of SnO_2 and ZnO was obtained with ZnO as the dominant phase. While the reaction was performed in EG (Fig. 3c), only cubic-phase $ZnSn(OH)_6$ (JCPDS 73-2384) was produced. It appears that, under the present reaction condition, only in W/EG mixed solvent ZTO can be successfully synthesized (Fig. 3b).

The foregoing discussion indicates that ZnO and SnO_2 are apt to be formed in low temperature and low *n*-butylamine concentration, respectively. When water was used as the solvent, the formation of ZnO and SnO_2 suggests that the current hydrothermal temperature and/or *n*-butylamine concentration is not high enough to form ZTO in water. As we known, EG is a neutral solvent with two −OH bonds and is generally referred to as a capping material [21]. It could link to the surface of crystallites via either covalent bonds or dative bonds. When a certain quantity of EG was introduced into the water solution, two complexing agents $Zn(OH)_4^{2-}(EG)_x$ and $Sn(OH)_6^{2-}(EG)_y$ can be formed [21,22] (the *x*, *y* value depending on the concentration of EG [23]). These two agents adsorb to ZnO nuclei (the main resultant in water) and thus decrease its surface energy [24], which facilitates the reaction of Eq. (7) and produces ZTO. When the reaction performed in EG solution, for the lack of water, Zn^{2+} and Sn^{4+} will react with the EG molecules to form two coordination complexes of $Zn^{2+}(EG)_x$ and $Sn^{4+}(EG)_y$. These two complexes react with OH^- (dissociated from the water coming from $SnCl_4 \cdot 5H_2O$ or impurity water of EG solvent) during the following hydrothermal process and form $ZnSn(OH)_6$ (Eq. (8)). $ZnSn(OH)_6$ is a metastable intermediate phase and can be

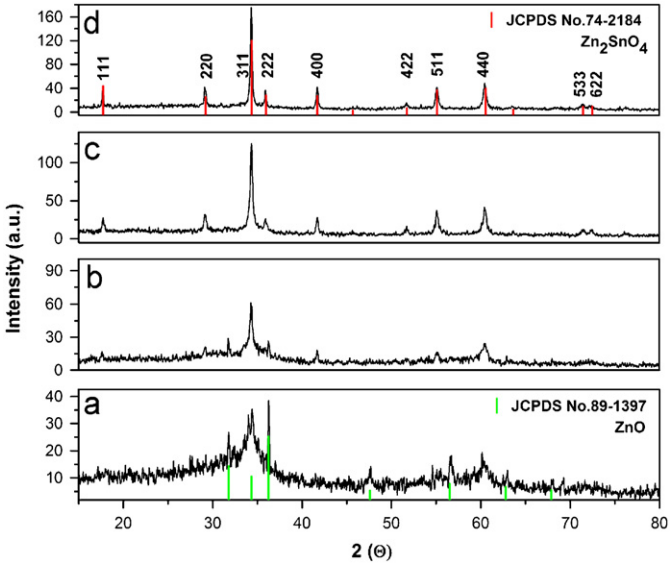

Fig. 2. XRD patterns of the samples synthesized at different temperature: (a) 140 °C, (b) 160 °C, (c) 180 °C, and (d) 200 °C (solvent: W/EG, amine: 0.4 M *n*-butylamine, time: 20 h).

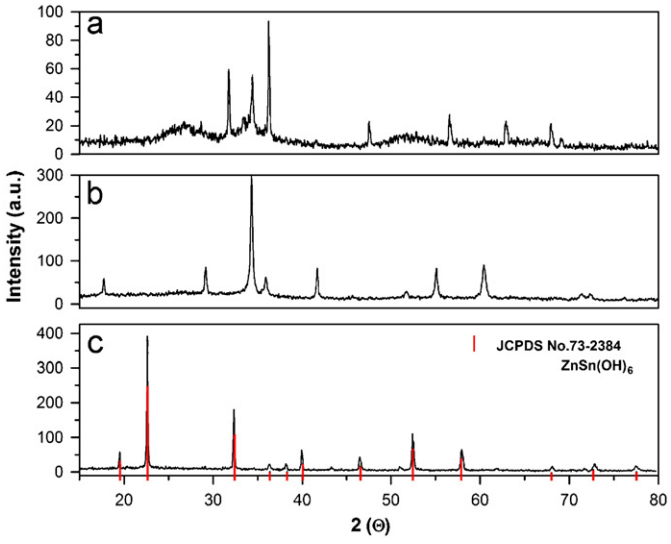

Fig. 3. XRD patterns of the samples synthesized in different solvent: (a) H_2O, (b) W/EG, and (c) ethylene glycol (temperature: 180 °C, time: 20 h, amine: 0.4 M *n*-butylamine).

stabilized by further capping of EG to form $ZnSn(OH)_6(EG)_z$, which at last retards the transformation of $ZnSn(OH)_6$ to ZTO.

$$Zn(OH)_4^{2-}\ (EG)_x + ZnO + Sn(OH)_6^{2-}\ (EG)_y \rightarrow Zn_2SnO_4\downarrow + (x+y)\ EG + 4OH^- + 3H_2O \quad (7)$$

$$Zn^{2+}\ (EG)_x + Sn^{4+}\ (EG)_y + 6OH^- \rightarrow (x+y)\ EG + ZnSn(OH)_6 \rightarrow ZnSn(OH)_6\ (EG)_z \quad (8)$$

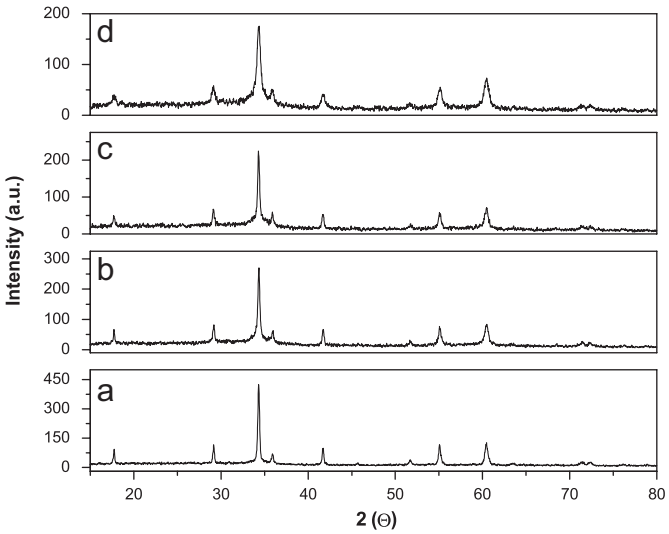

Fig. 4. XRD patterns of the samples synthesized in 0.53 M amines solution: (a) ZTO-e (ethylamine), (b) ZTO-b (*n*-butylamine), (c) ZTO-h (*n*-hexylamine), and (d) ZTO-o (*n*-octylamine) (solvent: W/EG, temperature: 180 °C, time: 20 h).

3.1.4. *Effect of the kind of amine*

Besides *n*-butylamine, ethylamine, *n*-hexylamine, and *n*-octylamine were also chosen as the mineralizer. Since their pK_b values are almost the same as *n*-butylamine ($pK_b = 3.36$) [25], the effect of their concentrations on the product structure should be similar to that of *n*-butylamine. Thus, in order to synthesize pure ZTO, the optimized amine concentration and hydrothermal temperature were 0.53 M and 180 °C, respectively. The validity of this reaction conditions was verified by pure ZTO phase shown in Fig. 4. (The corresponding ZTO samples are denoted as ZTO-e, ZTO-b, ZTO-h, and ZTO-o, respectively.) With the increase of the carbon chain length of the amines, the diffraction peaks intensities of the samples are decreased and the peaks become more broadened, which means the particle sizes become smaller. It seems that the crystallinity and particle size of the ZTO are inhibited by increasing the carbon chain length of the amines. In the hydrothermal synthesis of TiO_2, Ryu et al. also found that the TiO_2 particle size was suppressed by increasing the carbon chain length of amine [26].

3.2. *Morphology of ZTO synthesized in different amines*

The morphologies of the ZTO samples synthesized in different amine solutions were investigated by SEM (Fig. 5) and TEM (Fig. 6). In "small" amines solutions, such as ethytlamine (Fig. 5a) and *n*-butylamine solution (Fig. 5b), the small nanosized ZTO particles tend to aggregate and grow to larger particles, while in *n*-hexylamine (Fig. 5c) and *n*-octylamine (Fig. 5d) solutions the particle sizes become smaller and more uniform. These observations are consistent with the speculation arising from the XRD patterns in Fig. 4. Interestingly, the ZTO particles obtained in *n*-butylamine solution are faceted hexagonal-shape crystal (denoted as H-ZTO), attached with many small irregular crystallites. After ultrasonic dispersion, the hexagonal structure becomes

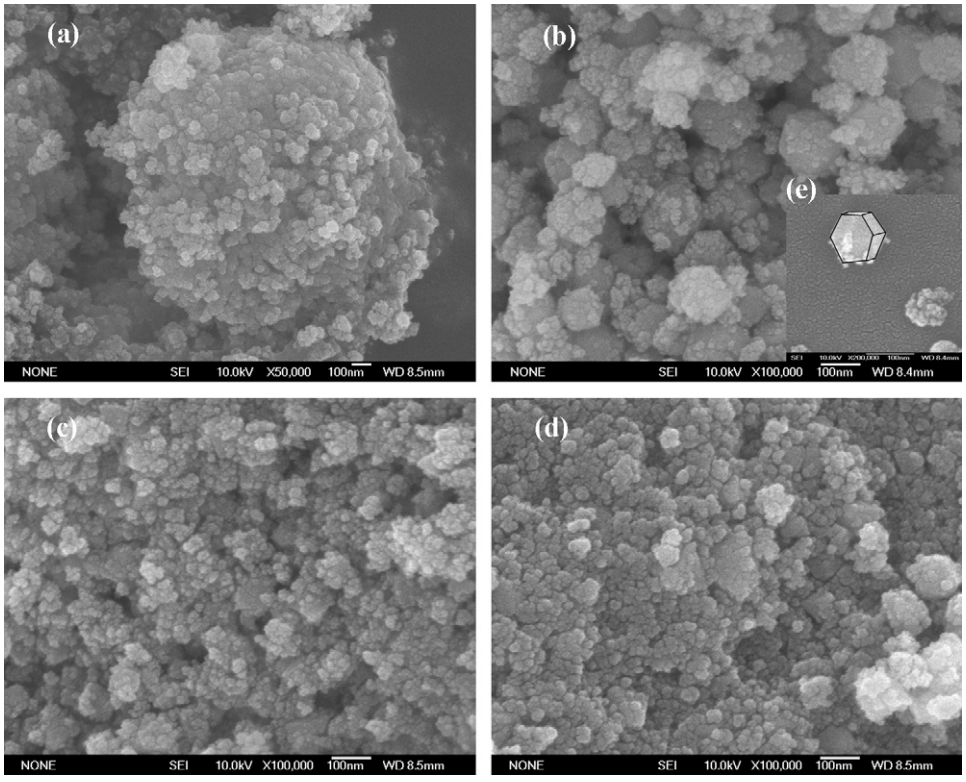

Fig. 5. SEM images of the ZTO synthesized at different kind of amines solutions: (a) ethylamine, (b) and (e) *n*-butylamine, (c) *n*-hexylamine, and (d) *n*-octylamine.

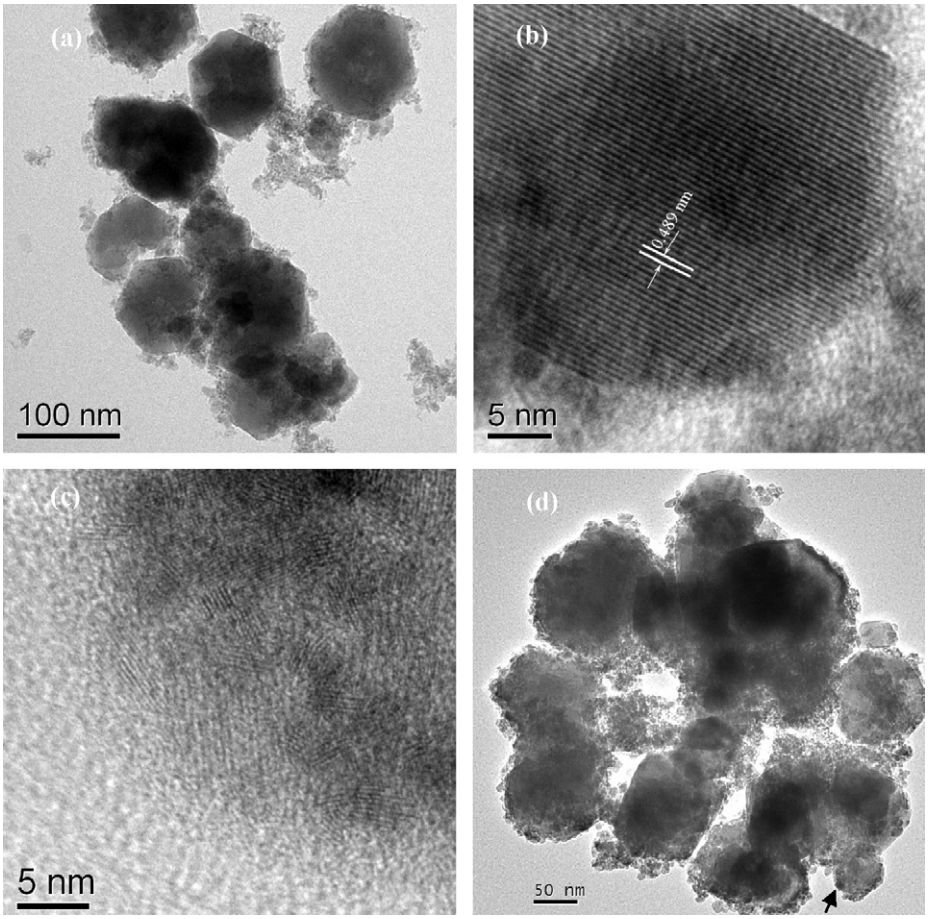

Fig. 6. TEM images of: (a) H-ZTO and (d) Pt modified H-ZTO; (b) and (c) HRTEM images of H-ZTO.

apparent (Fig. 5e). It is likely that these hexagonal particles are formed by adsorption of small irregular nanoparticles through the Ostwald ripening process. TEM image (Fig. 6a) further verifies the shape and reveals that the edge length of the hexagonal structure is in the range of 40–70 nm. The size of the attached nanoparticles is sub-5 nm (Fig. 6a and c). Lattice fringes with a d spacing of about 0.489 nm, corresponding to the {111} plane of the hexagonal structure are found in Fig. 6b. Fig. 6d shows the TEM image of Pt modified hexagonal-shaped ZTO (H-ZTO). But due to the difficulty of distinguishing the Pt particles from the attached nano-ZTO particles (sub-5 nm), it is hard to estimate the size and dispersion of Pt.

3.3. Optical properties of ZTO

The light absorption ability of H-ZTO sample was detected by UV–Vis DRS, as shown in Fig. 7. The steep shape of the spectra indicated that the light absorption was not due to the transition from the impurity level, but due to the band gap transition. The optical band gap of H-ZTO can be derived using Tauc's formula $(ahv)^{1/n} = (hv - E_g)$ [27], where α is the absorption coefficient and hv is the photon energy. As ZTO is a direct semiconductor, n is equal to 1/2 [17]. The insert of Fig. 7 shows the plot of $(\alpha hv)^2$ versus hv. Clearly, the as-prepared H-ZTO sample has a band gap of 3.7 eV, which is a little higher than the reported bulk ZTO value of 3.6 eV [28]. The increase in the band gap may be originated from the size quantum effects of the attached nanoparticles because the size of them is sub-5 nm (indicated by the TEM image), much smaller than bulk ZTO. A similar observation of nano-ZTO has been reported by other groups [15,17].

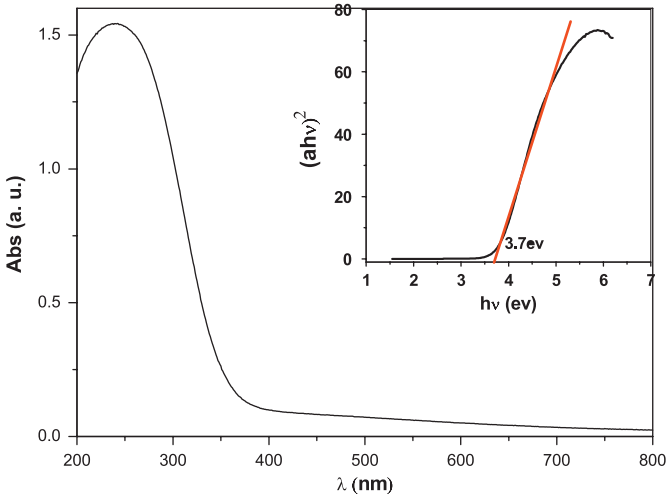

Fig. 7. Diffuse reflectance adsorption spectra of H-ZTO. The insert showed the plots of $(\alpha hv)^2$ versus the energy of light hv.

The PL spectrum of H-ZTO was measured at room temperature, as shown in Fig. 8. When the sample was excited with 280 nm light, a broad strong green emission with a band centered at 550 nm could be observed. Similar results have been obtained by other investigators [29,30]. Obviously, this emission peak is not the band-to-band emission for the band gap of H-ZTO is 3.7 eV. In the previous investigations of the semiconductor nanomaterials (such as: ZnO, SnO_2), the green emission is often attributed to

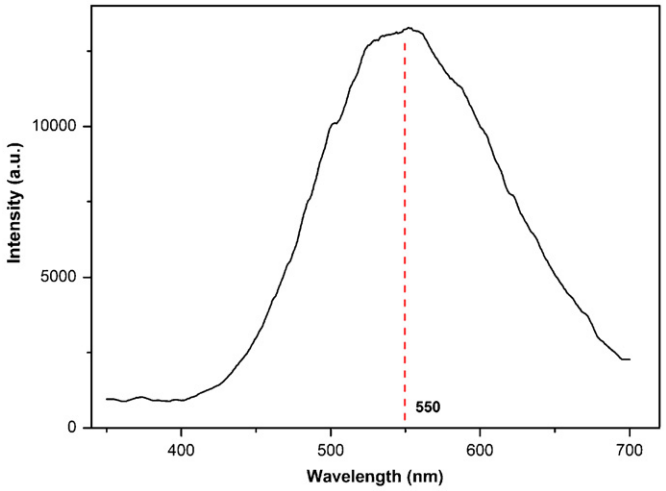

Fig. 8. PL spectra of H-ZTO excited at 280 nm under room temperature.

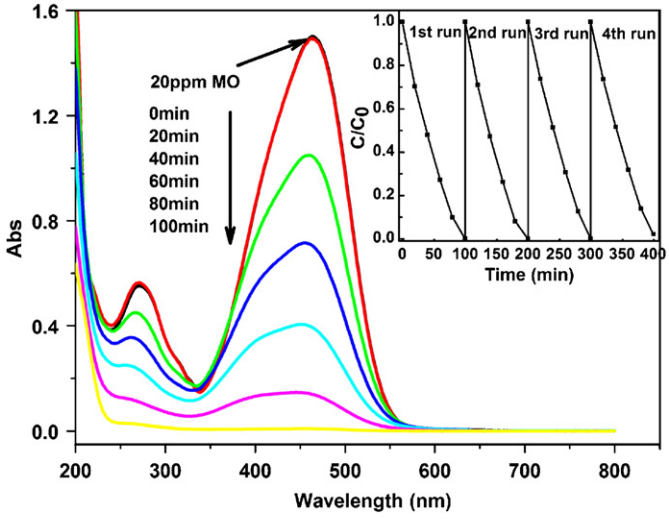

Fig. 9. Temporal band changes in absorption spectra during the photodegradation of 200 mL MO solution (20 ppm) in the presence of 50 mg ZTO (synthesized in 0.4 M *n*-butylamine solution at 180 °C for 20 h). The insert shows the profiles of cyclic tests of the reaction.

oxygen vacancies [31]. As for the H-ZTO sample, the strong green emission is probably owing to the similar luminescent center, which might be formed in the hydrothermal process [32]. In addition, the H-ZTO nanoparticles with high surface-to-volume ratio should also favor the existence of large quantities of oxygen vacancies [30]. These oxygen vacancies induce the formation of new energy levels in the band gap of H-ZTO. The recombination of a photo-excited hole with an electron occupying an oxygen vacancy yields the green emission.

3.4. Photocatalytic activity

3.4.1. Photodegradation of MO

The changes of the absorption peaks during the photodegradation of MO in the presence of ZTO (synthesized in 0.4 M *n*-butylamine solution at 180 °C for 20 h) are displayed in Fig. 9. It is observed that approximately 0.5% MO was adsorbed by the ZTO particles after stirring in the dark for 60 min (compare the spectra of "20 ppm MO" and "0 min" in Fig. 9). This result suggests that the adsorption of MO onto ZTO is neglectable. After illuminating with 254 nm UV light for 100 min, no MO was detectable in the

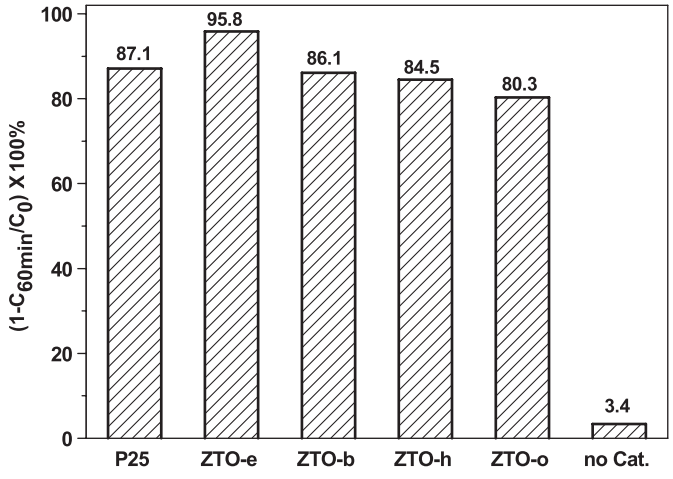

Fig. 10. The decolorization rates of MO over different ZTO samples synthesized in different amines solutions. C_o and $C_{60\,min}$ are the equilibrium concentration of MO before and after UV irradiation for 60 min, respectively.

solution. The stability of the activity was evaluated by cyclic experiments. The reactions were carried out under the same experiment conditions. After each reaction, 20 mL of 200 ppm MO aqueous solution was added to the reactor to make up the volume loss caused by analyzing and regenerate the solution. The catalysts containing in the former analyzing samples was reused. The result shown in the insert of Fig. 9 reveals that little deactivation was observed after four cycles.

The photocatalytic activity of ZTO synthesized in different amines was compared in Fig. 10 by the degradation of MO. In the absence of photocatalyst, only 3.4% MO was decomposed after 1 h irradiation, indicating that MO is photo-stable. The activities of the samples are decreased in the order ZTO-e (95.8%) > ZTO-b (86.1%) > ZTO-h (84.5%) > ZTO-o (80.3%). The ZTO-e sample exhibits highest decolorization rate, even better than Degussa P25 (87.1%).

The BET surface areas of the series of ZTO samples are 63.05 (ZTO-e), 70.73 (ZTO-b), 78.94 (ZTO-h), and 93.22 m^2/g (ZTO-o), respectively. Although the surface areas of the ZTO samples are enhanced by using long carbon chain amines, the photoactivities are not improved accordingly. Inversely, the activities are somewhat reduced. Highly crystallized particles had been considered to favorably decrease the probability of electron–hole recombination and consequently showed enhanced photoactivity [33,34]. The decrease of the activities may be also due to the lower crystallinities of the ZTO samples, which has been shown in Fig. 4.

3.4.2. Photocatalytic H_2 production

Fig. 11 demonstrates the time course of the photocatalytic H_2 production from ethanol solution over P25 and H-ZTO. The addition of platinum to photocatalyst particles has been shown to enhance the photocatalytic activity, particularly the activity of producing hydrogen from H_2O [35]. An attempt to improve the efficiency of H-ZTO was also made by modification with platinum. It is found that the formation rates of H_2 evolution over H-ZTO (Fig. 11b) and Pt modified H-ZTO (Fig. 11c) are much larger than that of P25 (Fig. 11a). For naked H-ZTO the hydrogen evolution rate improved slowly at the first 6 h and then remained constant of about 0.231 mmol/h. Long time catalytic tests show that no apparent deactivation occurred over 33 h. The improvement of the hydrogen evolution rate at the first 6 h can be attributed to the increasing dispersion of ZTO particles by stirring because there are many small irregular crystallites attached to the hexagonal-shaped particles. If a pre-stirred sample was used, the time to

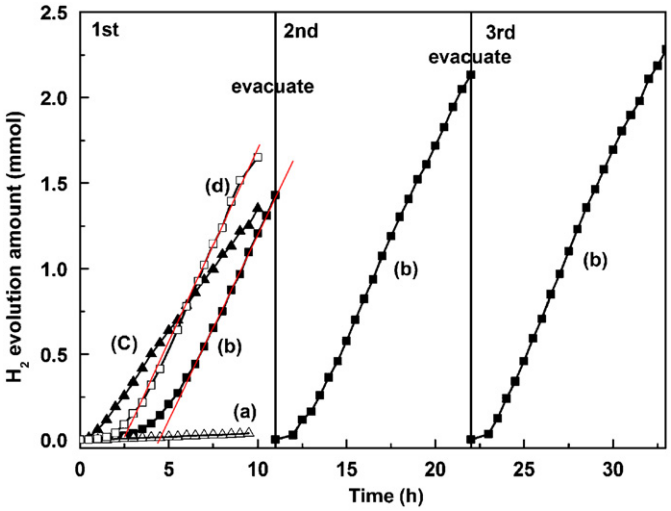

Fig. 11. Photocatalytic H_2 production from ethanol solution (195 mL water, 5 mL C_2H_5OH) over 50 mg: (a) P25, (b) H-ZTO, (c) Pt (1 wt%) modified H-ZTO, and (d) the H-ZTO sample which has been pre-stirred in 195 mL water for 5 h.

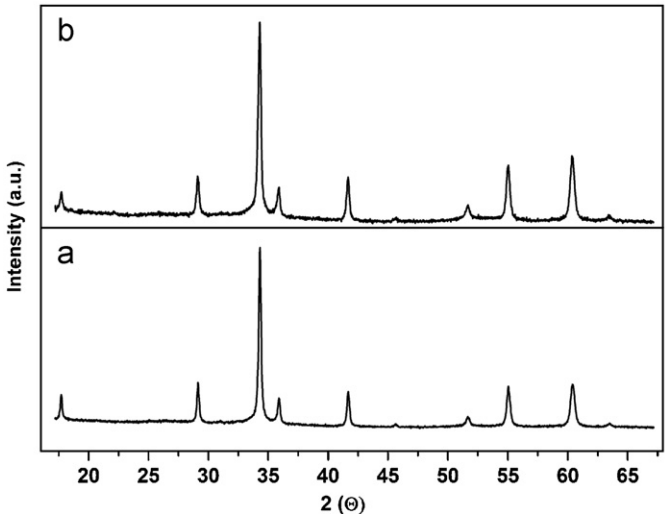

Fig. 12. XRD patterns of the H-ZTO: (a) before and (b) after H_2 evolution reaction.

reach the constant H_2 evolution rate would be reduced. In order to validate this claim, a verification experiment is conducted after the H-ZTO sample has been pre-stirred in 195 mL water for 5 h. As shown in Fig. 11d, the hydrogen evolution rate increases more rapidly than the un-pre-stirred sample and only needs 2.5 h to reach the constant rate of 0.231 mmol/h. In contrast to most reports, the hydrogen evolution rate of H-ZTO is not improved by modification with 1 wt% Pt. Inversely, the hydrogen evolution rate decreases from 0.231 to 0.145 mmol/h. A similar phenomenon has been observed on ZrO_2 by Sayama et al. [36].

Commonly, platinization does not significantly change the physical properties of the photocatalyst such as surface area, crystalline phase composition, and particle size [20]. But the addition of Pt can change the surface properties of semiconductor by the formation of a Schottky barrier because the work function of Pt is usually larger than that of semiconductor. The presence of the Schottky barrier can decrease the recombination of photo-generated electron–hole pairs, consequently prolonging their lifetime, and greatly enhancing the photocatalytic activity [37]. For our sample, the XRD and BET data of Pt modified H-ZTO have no apparent differences compared to H-ZTO. The UV–Vis DRS of platinized H-ZTO and H-ZTO show no significant differences in the UV range, but due to its dark grey color, platinized sample shows a stronger adsorption respect to unmodified sample throughout the visible range. Therefore the decrease of the hydrogen evolution rate caused by the changes of these parameters can be ignored. The work function of ZTO is reported to be as high as 5.3 eV [38,39], very close to the value of Pt 5.36 eV [40]. This high work function will unfavor the formation of Schottky barrier. Furthermore, non-ohmic contact has been found between Pt and ZTO [41]. These two factors suggest that the photoelectrons will be difficult to migrate from ZTO to Pt. This may be the reason why the activity of H-ZTO was not improved by loading of Pt.

Fig. 12 shows the XRD patterns of the sample before and after the H_2 evolution reaction. There are no apparent changes, indicating that the synthesized ZTO is stable in the present reactions.

4. Conclusions

Nanosized spinel-type ZTO was synthesized by the hydrothermal process using amines (ethylamine, *n*-butylamine, *n*-hexylamine, and *n*-octylamine) and mixed solution (W/EG) as alkaline mineralizer and reaction solvent, respectively. For *n*-butylamine, only the reaction temperature is above 180 °C and *n*-butylamine concentration is larger than 0.40 M, pure ZTO could be synthesized and the crystallinity of the ZTO was enhanced by hydrothermal treatment at high temperature and high *n*-butylamine concentration. The particle sizes and crystallinities of the ZTO synthesized in different amine solutions were hindered by increasing the carbon chain length of amines. A H-ZTO sample was prepared with 0.53 M of *n*-butylamine solution at 180 °C for 20 h and its band gap was found to be 3.7 eV by estimating from UV–Vis DRS. The PL spectrum showed that this hexagonal-shaped sample exhibited a broad strong green emission at 550 nm. The synthesized ZTO samples showed high activity and durability for photodegradation of MO and the activity is affected by the crystallinities of the samples. The H-ZTO showed much higher activity than P25 for photocatalytic production H_2 from ethanol solution. Modification with 1 wt% Pt did not improve the sample's activity.

Acknowledgments

This work was financially supported by the National Natural Science Foundation of China (Grant nos. 20673020, 20573020, and 20537010), the grants from Fujian Province (Grant nos. 2006F5057), and National Basic Research Program of China (973 Program, no. 2007CB613306). We are grateful to Professors Zhang Hanhui and Sun Ruiqing for use of their Photoluminescence facilities.

References

[1] B. Tan, E. Toman, Y.G. Li, Y.Y. Wu, J. Am. Chem. Soc. 129 (2007) 4162–4163.
[2] I. Stambolova, K. Konstantinov, D. Kovacheva, P. Peshev, T. Donchev, J. Solid State Chem. 128 (1997) 305–309.
[3] J.H. Yu, G.M. Choi, Sens. Actuator B 72 (2001) 141–148.
[4] F. Belliard, P.A. Connor, J.T.S. Irvine, Solid State Ionics 135 (2000) 163–167.
[5] A. Rong, X.P. Gao, G.R. Li, T.Y. Yan, H.Y. Zhu, J.Q. Qu, D.Y. Song, J. Phys. Chem. B 110 (2006) 14754–14760.
[6] X.D. Lou, X.H. Jia, H.Q. Xu, S.Z. Liu, Q.H. Gao, Mater. Sci. Eng. A 432 (2006) 221–225.
[7] W. Cun, X.M. Wang, J.C. Zhao, B.X. Mai, G.Y. Sheng, P.A. Peng, J.M. Fu, J. Mater. Sci. 37 (2002) 2989–2996.
[8] S. Wang, Z. Yang, M. Lu, Y. Zhou, G. Zhou, Z. Qiu, S. Wang, H. Zhang, A. Zhang, Mater. Lett. 61 (2007) 3005–3008.

[9] H.Y. Chen, J.X. Wang, H.C. Yu, H.X. Yang, S.S. Xie, J.Q. Li, J. Phys. Chem. B 109 (2005) 2573–2577.
[10] J.S. Jie, G.Z. Wang, X.H. Han, J.P. Fang, Q.X. Yu, Y. Liao, B. Xu, Q.T. Wang, J.G. Hou, J. Phys. Chem. B 108 (2004) 8249–8253.
[11] M.L. Zhang, T.C. An, X.H. Hu, C. Wang, G.Y. Sheng, J.M. Fu, Appl. Catal. A 260 (2004) 215–222.
[12] G. Fu, H. Chen, Z.X. Chen, J.X. Zhang, H. Kohler, Sens. Actuator B 81 (2002) 308–312.
[13] A. Kurz, K. Brakecha, J. Puetz, M.A. Aegerter, Thin Solid Films 502 (2006) 212–218.
[14] N. Nikolic, Z. Marinkovic, T. Sreckovic, J. Mater. Sci. 39 (2004) 5239–5242.
[15] H.L. Zhu, D.R. Yang, G.X. Yu, H. Zhang, D.L. Jin, K.H. Yao, J. Phys. Chem. B 110 (2006) 7631–7634.
[16] J. Fang, A.H. Huang, P.X. Zhu, N.S. Xu, J.Q. Xie, J.S. Chi, S.H. Feng, R.R. Xu, M.M. Wu, Mater. Res. Bull. 36 (2001) 1391–1397.
[17] J. Zeng, M.D. Xin, K.W. Li, H. Wang, H. Yan, W.J. Zhang, J. Phys. Chem. C 112 (2008) 4159–4167.
[18] M.R. Hoffmann, S.T. Martin, W.Y. Choi, D.W. Bahnemann, Chem. Rev. 95 (1995) 69–96.
[19] Z.G. Zou, J.H. Ye, K. Sayama, H. Arakawa, Nature 414 (2001) 625–627.
[20] M.C. Hidalgo, M. Maicu, J.A. Navio, G. Colon, Catal. Today 129 (2007) 43–49.
[21] T. Ghoshal, S. Kar, S. Chaudhuri, Cryst. Growth Des. 7 (2007) 136–141.
[22] M.M. Bagheri-Mohagheghi, N. Shahtahmasebi, M.R. Alinejad, A. Youssefi, M. Shokooh-Saremi, Physica B 403 (2008) 2431–2437.
[23] L.M. Yang, Y.L. Su, Y.Z. Xu, S.W. Zhang, J.G. Wu, K. Zhao, J. Inorg. Biochem. 98 (2004) 1251–1260.
[24] Q. Xiao, Powder Technol., 2008, doi:10.1016/j.powtec.2008.06.008.
[25] D.R. Lide (Ed.), CRC Handbook of Chemistry and Physics, 85th ed, CRC Press, Boca Raton, 2005.
[26] Y.B. Ryu, M.S. Lee, E.D. Jeong, H.G. Kim, W.Y. Jung, S.H. Baek, G.-D. Lee, S.S. Park, S.-S. Hong, Catal. Today 124 (2007) 88–93.
[27] D.L. Wood, J. Tauc, Phys. Rev. B 5 (1972) 3144.
[28] T.J. Coutts, D.L. Young, X. Li, W.P. Mulligan, X. Wu, J. Vac. Sci. Technol. A 18 (2000) 2646–2660.
[29] Y. Su, L.-A. Zhu, L. Xu, Y. Chen, H. Xiao, Q. Zhou, Y. Feng, Mater. Lett. 61 (2007) 351–354.
[30] J.X. Wang, S.S. Xie, Y. Gao, X.Q. Yan, D.F. Liu, H.J. Yuan, Z.P. Zhou, L. Song, L.F. Liu, W.Y. Zhou, G. Wang, J. Cryst. Growth 267 (2004) 177–183.
[31] F.H. Leiter, H.R. Alves, A. Hofstaetter, D.M. Hofmann, B.K. Meyer, Phys. Status Solidi B 226 (2001) R4–R5.
[32] Y. Sun, N. George Ndifor-Angwafor, D. Jason Riley, M.N.R. Ashfold, Chem. Phys. Lett. 431 (2006) 352–357.
[33] K.Y. Jung, S.B. Park, J. Photochem. Photobiol. A. 127 (1999) 117–122.
[34] A. Testino, I.R. Bellobono, V. Buscaglia, C. Canevali, M. D'Arienzo, S. Polizzi, R. Scotti, F. Morazzoni, J. Am. Chem. Soc. 129 (2007) 3564–3575.
[35] F.E. Osterloh, Chem. Mater. 20 (2008) 35–54.
[36] K. Sayama, H. Arakawa, J. Phys. Chem. 97 (1993) 531–533.
[37] A.L. Linsebigler, G.Q. Lu, J.T. Yates, Chem. Rev. 95 (1995) 735–758.
[38] G. Guzman, B. Dahmani, J. Putz, M. Aegerter, J. Puetz, M.A. Aegerter, US2004113146-A1.
[39] T. Minami, J. Vac. Sci. Technol. A 17 (1999) 1765–1772.
[40] H. Suzuki, T. Sato, K. Kamitsuji, S. Kaneko, H. Kawasaki, C. Kaito, J. Cryst. Growth 268 (2004) 238–241.
[41] J.H. Yu, G.M. Choi, J. Electrochem. Soc. 148 (2001) G307–G314.